J. Fluid Mech. (2016), *vol.* 800, *pp.* 248–263.
doi:10.1017/jfm.2016.384

Lift on side-by-side intruders within a granular flow

R. A. López de la Cruz[1] **and G. A. Caballero-Robledo**[1,†]

[1]CINVESTAV-Monterrey, PIIT, Nuevo León, 66600, México

(Received 4 December 2015; revised 6 April 2016; accepted 2 June 2016;
first published online 1 July 2016)

For the first time, we used computer simulations to study lift forces on two static disks placed side-by-side within a two-dimensional granular flow and found them to be either repulsive or attractive depending on the flow velocity and separation between the disks. Our simulations results reveal that differences in the flow velocity between the disks and outside of that region are closely correlated with the lift force. We propose an empirical function for the lift force based on this correlation and our dimensional analysis. The specific region where the measured velocity exhibits this correlation suggests that attractive lift is not a Bernoulli-like effect. Instead, we speculate that it might be explained by a force balance based on Coulomb's theory of passive failure in a Mohr–Coulomb material. Our results confirm that repulsive lift is due to the jamming of particles flowing between the disks.

Key words: complex fluids, granular media, granular mixing

1. Introduction

Historically, studying the drag and lift forces on objects immersed in fluids has been an excellent way to advance the theory and application of fluid mechanics. The flow around objects immersed within granular flows is also extremely instructive for understanding the essential features of the mechanics of granular matter (Wieghardt 1975; Albert *et al.* 1999; Chehata, Zenit & Wassgren 2003; Geng & Behringer 2005; Caballero-Robledo & Clément 2009; Ding, Gravish & Goldman 2011; Seguin *et al.* 2011; Guillard, Forterre & Pouliquen 2013, 2014).

Interest in granular matter by the scientific community has mainly focused on the study of the drag force on objects immersed in a granular medium. Only recently have lift forces attracted attention (Zuriguel *et al.* 2005; Nelson *et al.* 2008), especially in the context of locomotion in sand, which has applications in biomechanics and robotics (Ding *et al.* 2011; Goldman 2014).

The drag force on an intruder immersed in a stationary flow has been thoroughly studied, both with a static object immersed in a flow of moving grains (Wieghardt 1975; Albert *et al.* 1999; Chehata *et al.* 2003; Geng & Behringer 2005; Seguin *et al.* 2011), and with an object moving at a constant velocity in a static granular medium (Ding *et al.* 2011; Guillard *et al.* 2013, 2014). The consensus is that the drag force is independent of velocity in slow flow, while in fast flows the drag force changes

† Email address for correspondence: g.a.caballero.robledo@gmail.com

linearly with the square of the flow velocity. The former is a quasistatic regime where friction and gravity dictate the dynamics, while the latter is an inertial regime (Faug 2015).

Concerning lift force, Ding *et al.* (2011) recently showed the existence of upward lift forces on objects dragged horizontally in a granular medium. The lift force depends on the shape of the object and is due to the asymmetry in pressure caused by gravity between the upper and lower parts of the object. The authors successfully modelled the stresses on the object using Coulomb's theory of passive failure in a Mohr–Coulomb material.

Objects immersed in fluids can also interact with other objects through hydrodynamic interactions even if they are not in contact. The interaction of sedimenting or rising pairs of particles side-by-side in a fluid is a classical set-up, which is nevertheless not easy to describe analytically or to study experimentally (Wijngaarden & Jeffrey 1976; Kim, Elghobashi & Sirignano 1993; Wu & Manasseh 1998; Legendre, Magnaudet & Mougin 2003; Vélez-Cordero *et al.* 2011). Kim *et al.* (1993) numerically simulated the interaction of two solid spheres placed side-by-side at low Reynolds numbers (<150) and found that they repel each other when they are close together, with a repulsion which grows with proximity. The two spheres attract each other at intermediate distances and any lift, together with any other interaction, vanishes for $X_{sep}/D > 20$, where X_{sep} is the size of the gap between the two spheres and D is the diameter of the spheres. Drag on the spheres is found to increase when $X_{sep}/D < 3$.

Intruders immersed in granular media also interact with those that are far away. In the context of granular materials, long-range interactions become especially relevant for understanding the complex phenomenology of granular segregation: when a mixture of different species of grains is agitated or forced to flow in specific conditions, the grains of each species group together and segregate from the rest. This phenomenon can have important implications for areas such as soil mechanics and in mining, pharmaceuticals and food industry applications (Ottino & Khakhar 2000; Aumaître, Kruelle & Rehberg 2001; Sanders *et al.* 2004; Zuriguel *et al.* 2005; Cattuto *et al.* 2006; Shaebani, Sarabadani & Wolf 2012). Another area for which segregation is crucial is geophysics, as reported by studies on increased avalanche mobility caused by segregation (Moro *et al.* 2010).

Local velocity fluctuations have been reported as being responsible for the attraction between intruders immersed in an agitated granular medium (Aumaître *et al.* 2001; Zuriguel *et al.* 2005; Cattuto *et al.* 2006; Shaebani *et al.* 2012), while local flow velocity and a Bernoulli-like effect have been associated with the attraction (Pacheco-Vazquez & Ruiz-Suarez 2010; Solano-Altamirano *et al.* 2013) and repulsion (Zuriguel *et al.* 2005) of intruders within granular flows.

In a previous work by our group (Solano-Altamirano *et al.* 2013) we sought to unravel the mechanisms behind the attraction and repulsion between heavy disks, as they impact and penetrate a quasi-two-dimensional superlight granular medium (Pacheco-Vazquez & Ruiz-Suarez 2010). By combining experiments and computer simulations, we found that the flow in the gap between the intruders was always faster than on their other sides, but the attraction existed only if the intruders were penetrating at a speed greater than ~ 1 m s^{-1}. However, in such impact experiments, many variables change continuously with time, including the speed, separation and depth of the intruders. This makes it extremely difficult to understand the origins of attractive and repulsive lifts.

We present here numerical simulations of a new version of this set-up, wherein the intruders are kept fixed while the granular medium flowing around them is driven by

gravity. This allows for the measurement of the forces on the intruders in a stationary situation, and by systematically varying the intruders' separation and the flow velocity, we identified regimes characterized by attractive and repulsive lifts. We were able to reproduce the lift force for different local flow velocities on both sides of the intruders, and propose an empirical formula for the lift force, which reveals that the origin of the attraction or repulsion is not a Bernoulli-like effect. However, our simulations are two-dimensional and the size of our system turned out to be much smaller than the range of interaction between intruders, so it is not necessarily true that the results presented here would be reproduced in an experiment. That is why we are currently developing an experimental set-up for which the preliminary results also show these attraction and repulsion regimes, which we will report on a follow-up paper, together with computer simulations in three dimensions and in much larger systems using parallel computing with graphics processing units.

Our set-up represents the granular version of a classical set-up that has been thoroughly studied in fluid mechanics (Wijngaarden & Jeffrey 1976; Kim *et al.* 1993; Legendre *et al.* 2003; Vélez-Cordero *et al.* 2011). It is, in fact, surprising that it has not been applied to granular flow until now.

2. Simulation implementation

Simulations were implemented using the discrete element method for soft particles in two dimensions, which allows long-lasting multiple contacts between the particles. The original code was developed by Wassgren (1996) and was adapted to include periodic boundary conditions in the vertical dimension. Our numerical code considers only the contact forces and gravity. For the normal component of the contact forces, we used a model proposed by Walton & Braun (1986). In this model, the normal contact force during a contact on a particle i due to another particle j, $\boldsymbol{F}_N^{ij}$, is modelled using a linear spring during loading, and another linear, but stiffer, linear spring during unloading:

$$\boldsymbol{F}_N^{ij} = \begin{cases} -k_l \delta \hat{\boldsymbol{n}} & \text{loading} \\ -k_u(\delta - a_0)\hat{\boldsymbol{n}} & \text{unloading,} \end{cases} \tag{2.1}$$

where k_l (k_u) is the loading (unloading) spring constant, δ is the overlap between particles, $\hat{\boldsymbol{n}}$ is the unit vector normal to the contact and a_0 is the overlap at which the unloading force is zero due to the plastic deformation of the particles. For each pair of particles in a specific contact, $a_0 = \delta_{max}(k_u - k_l)/k_u$, where δ_{max} is the maximum overlap for that contact: whenever $\delta \leqslant a_0$ the contact finishes. With these considerations, the coefficient of restitution is

$$\varepsilon = \sqrt{\frac{k_l}{k_u}}. \tag{2.2}$$

The tangential force, $\boldsymbol{F}_S^{ij}$, is modelled as a Coulombic sliding friction element in series with a linear tangential spring (Cundall & Strack 1979):

$$\boldsymbol{F}_S^{ij} = -\min(\mu|\boldsymbol{F}_N^{ij}|, k_t|\boldsymbol{\gamma}|)\frac{\boldsymbol{\gamma}}{|\boldsymbol{\gamma}|}, \tag{2.3}$$

where μ is the coefficient of sliding friction, k_t is the tangential spring constant, $\boldsymbol{\gamma} = \gamma\hat{s}$ is the total tangential displacement and $\hat{s} = -n_y\hat{\imath} + n_x\hat{\jmath}$. The value of the tangential displacement is restricted to be smaller than the maximum value $\gamma_{\max} = \mu|\boldsymbol{F}_N^{ij}|/k_t$. The

	Grain–grain	Grain–disk	Grain–wall
k_l (kg s^{-2})	535	1649	50
k_u (kg s^{-2})	2140	3365	1263
k_t (kg s^{-2})	268	824	25
μ	0.5	0.7	0.5
ϵ	0.5	0.7	0.2

TABLE 1. Coefficients of friction μ and restitution ε, and stiffness of the springs used in the simulations.

stiffness of the tangential spring is determined as a fraction of the normal loading spring. In our case, $k_t/k_l = 0.5$.

The parameters of our simulations are shown in table 1 and they are the same as those used in a previous work by our group (Solano-Altamirano *et al.* 2013). In choosing these values we assumed that the macroscopic behaviour of the system was not sensitive to the precise value of the stiffness constants because that is what Wassgren (1996) found while simulating glass beads. However, we are now working with extremely light particles and such an assumption may no longer hold. It has been shown that when the normal contact stiffness is sufficiently large compared to a characteristic pressure of the system, the simulation is in the asymptotic limit of rigid grains and the macroscopic behaviour is insensitive to the stiffness value (Kneib *et al.* 2016). The simulation is in the limit of rigid grains whenever the dimensionless number $N_0 = k_n/P_0 d \geqslant 10^4$, where P_0 is a characteristic pressure of the system. In our case $N_0 \sim 6 \times 10^3$, which means that we are not in the limit of rigid grains, but we are not far from it. Although it will be interesting to study the effect of varying k_n on the macroscopic behaviour of our system, we believe that the current values of our parameters are reasonable since in our previous work we were able to quantitatively match our simulations with experimental results (Solano-Altamirano *et al.* 2013).

3. Simulation set-up

The system consists of a channel, delimited by a pair of vertical walls separated by distance L, and two static disks of diameter $D = 2.5$ cm, located side-by-side in the middle of the channel and separated from each other by a distance X_{sep} (see figure 1). We placed two staggered rows of small walls at the bottom of the channel, whose sizes can be varied, to allow for the control of the flow velocity U_∞ and to erase the flow memory. The second row of the small walls is useful to further break the memory of the granular medium. From these control walls and the periodic boundary conditions, long-lasting simulations and a homogenous velocity field along the channel are possible (see figure 1 in the supplementary material available at http://dx.doi.org/10.1017/jfm.2016.384).

In each simulation, we created 8000 grains with random initial radii, velocities and positions, which are left to settle under the effect of gravity. Initially, the grains are only a fraction of their final size to avoid overlap, and they grow with time until they reach an average diameter of $d = 0.52$ cm, with a size dispersion of 6 %. We simulated the grain material as polystyrene, with a mass density of $\rho_g = 0.014$ g cm^{-3} (for the sake of simplicity, we determined the density and mass of the grains as if the grains were spheres of diameter d, although the simulation is performed in two dimensions).

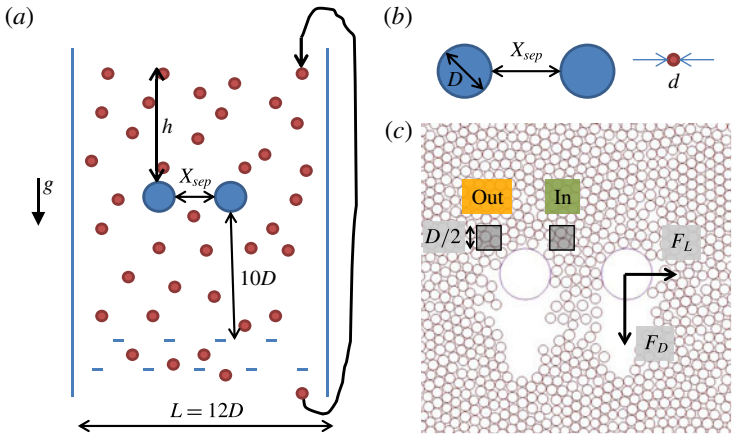

FIGURE 1. (Colour online) (*a*) Schematic representation of the simulation cell: a dense granular flow confined by lateral walls with periodic boundary conditions in the vertical direction. Small walls at the bottom of the cell control flow velocity and erase memory. (*b*) Intruders are static disks of diameter $D = 2.5$ cm, separated by a distance X_{sep}. The medium is composed of grains of diameter $d = 0.52$ cm. (*c*) Snapshot of the region around the intruders during flow. Positive lift and drag forces are defined, as are the 'in' and 'out' measurement regions.

The angle of repose of the simulated granular material was measured to be $\theta = 24.5°$, which corresponds to an effective friction coefficient of $\mu_{eff} = \tan(\theta) = 0.45$.

A wall, located at the bottom of the channel to contain the bed, is removed at time $t = 0$ s to begin the flow. The height of the column above the intruders stabilises at approximately $h \sim 33$ cm (see supplementary movies 1–6). Although h may vary, mainly because of the size of the voids behind the intruders, the variations are small and do not account for the change in drag and lift forces, which were found to depend linearly on h. We measured the lift force F_L and drag F_D on the intruders, whose positive directions are depicted in figure 1(*c*) for the right intruder. The mirror image of these forces correspond to the values for the left intruder. We systematically varied the flow velocity, $0.28 \leqslant U_\infty \leqslant 1.06$ m s^{-1}, and the separation between intruders, $1.25 \leqslant X_{sep} \leqslant 11.25$ cm, and for each configuration the simulation lasted approximately 7 s, with a simulation time step of 2.7×10^{-6} s. We registered force and position data at a rate of 21 717 samples per second which, for simulations of 7 s, makes the standard error of the mean of any averaged value to be extremely small. That is why in most of the plots the error is smaller than the symbol size.

4. Lift and drag

When the flow begins, the lift and drag forces exhibit a transient behaviour, which lasts for less than half a second, after which the forces stabilise and fluctuate around a well-defined average value (see figure 2*a*,*b*). Interestingly, the average lift force can be either attractive or repulsive, depending on the gap between the intruders and the flow velocity (figure 2*c*,*d*): a repulsive lift is associated with a small gap and high velocities. At intermediate separation distances, the lift becomes attractive, and reaches a minimum (maximum attraction), and tends to zero at larger X_{sep} values (we could not test greater separation distances to determine the exact range of intruder–intruder

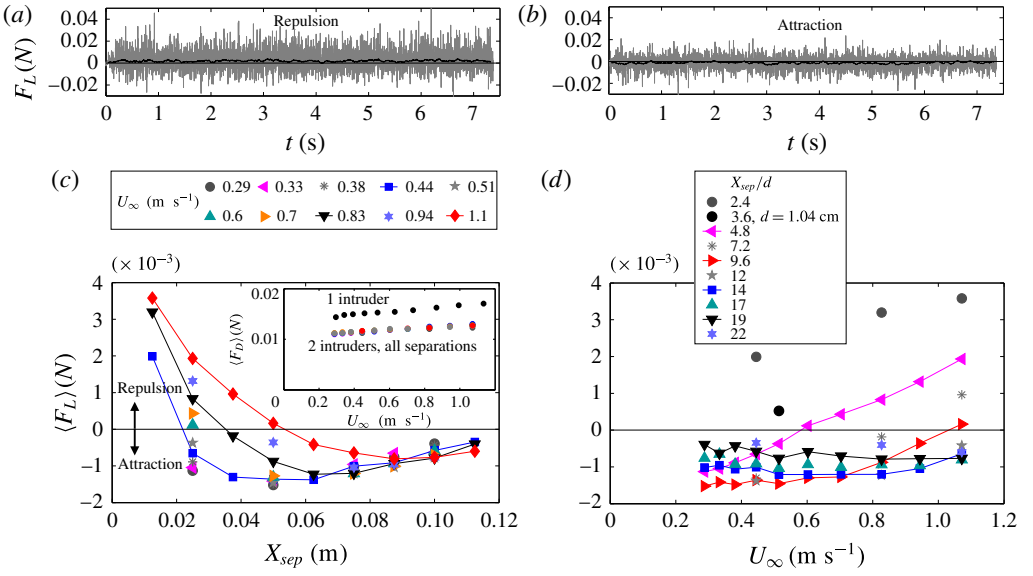

FIGURE 2. (Colour online) (*a*) and (*b*) Lift force on the right intruder as a function of time for a single simulation corresponding to, (*a*) $U_\infty = 1.1$ m s^{-1} and $X_{sep} = 2.5$ cm and (*b*) $U_\infty = 0.29$ m s^{-1} and $X_{sep} = 5$ cm. The thick black lines are sliding averages (with a time window of 0.05 s) showing attraction and repulsion. The force is registered at a rate of 21 717 samples per second. (*c*) Average lift force $\langle F_L \rangle$ as a function of intruders' separation X_{sep} for different flow velocities U_∞. Positive lift means repulsion. Inset: drag force as a function of U_∞. Drag is reduced when there are two intruders, but it does not depend on X_{sep}. (*d*) $\langle F_L \rangle$ as a function of U_∞ for intruders at different separation distances. The point with $X_{sep}/d = 3.6$ corresponds to a single simulation doubling the size of the grains, which suggests that the quantity X_{sep}/d is the relevant parameter concerning the lift force, although more simulations are needed to be conclusive on this point. The error bars (standard error of the mean) are smaller than the size of the symbols.

interactions because we did not want the distance from the intruders to the walls to be less than the size of the gap between the intruders). This behaviour reveals that there are two competing mechanisms involved in determining lift. Later, we demonstrate that repulsion results from the jamming of grains flowing between the intruders. In contrast, the origins of the attraction are not yet clear, but we can demonstrate that a Bernoulli-like effect is unlikely to explain either the attraction or repulsion, as has been suggested in other studies (Zuriguel *et al.* 2005; Pacheco-Vazquez & Ruiz-Suarez 2010; Solano-Altamirano *et al.* 2013).

The behaviour of the average drag force $\langle F_D \rangle$ is also interesting – compared to the drag that occurs with a single intruder, drag is reduced when there is another intruder placed alongside (see inset in figure 2*c*). Surprisingly, this drag reduction does not depend on the gap size between the intruders, at least not for the separation distances that we explored. This reflects the fact that the range of interaction of the two intruders is much larger than the lateral size of our container and therefore lateral confinement plays an important role. Indeed, lift and drag forces are very sensitive to variations in the distance L between the lateral walls (see figure 3*a*,*d*).

The inset in figure 2(*c*) shows that the drag force, on either one or two intruders, is almost constant despite variations in the flow velocity. This indicates that our system, even for the fastest flows, is a quasistatic regime dominated by friction and gravity,

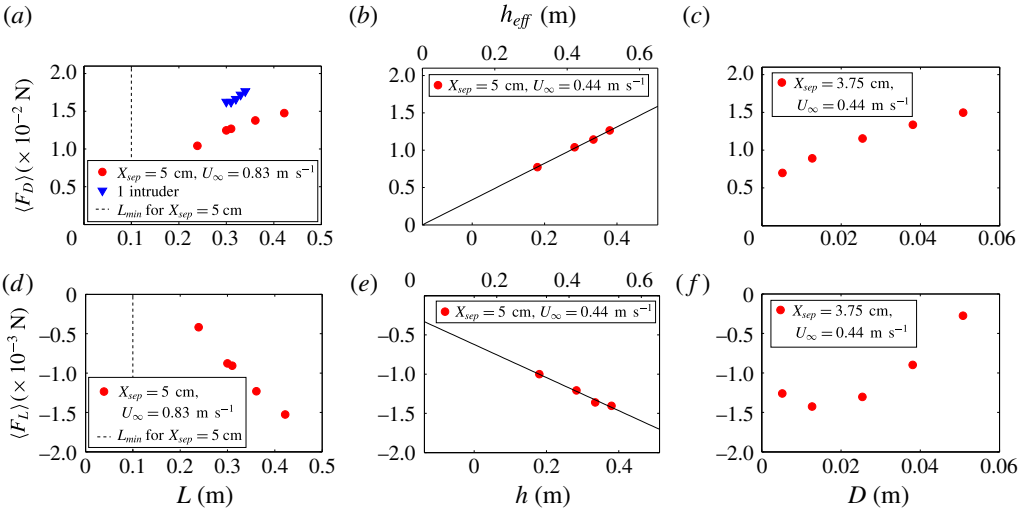

FIGURE 3. (Colour online) Average drag and lift forces versus L, h and D (defined in figure 1). The data in (*b*) and (*e*) are the only ones that follow a clear linear relation and we performed a linear fit. The quantity h_{eff} refers to the effective height of the column above the intruders due to the rain of grains impacting the surface of the granular column (see § 6). Simulations with smaller grain size d are very demanding computationally so we have only performed one simulation doubling the size of the grains for $X_{sep} = 3.75$ cm (see figure 2*d*).

in contrast with the inertial regime that is characterized by a dependence of the force on the square of the flow velocity (Faug 2015). However, although it is clear that our system is not in the inertial regime, the small variation of the drag force as a function of U_∞ indicates that it is not in a purely quasistatic regime either, where stresses are rate independent and can be described with Mohr–Coulomb friction models. Instead, this behaviour, which has been observed in other granular systems (Geng & Behringer 2005; Caballero-Robledo & Clément 2009; Kneib *et al.* 2016), seems to be consistent with the inertial rheology for sheared dense granular materials, where the bulk friction of the material is controlled by the non-dimensional inertia number $I = t_{micro}/t_{macro}$, where t_{micro} is a microscopic time scale related to rearrangements and t_{macro} is a macroscopic time scale related to shear rate (Andreotti, Forterre & Pouliquen 2013; Kneib *et al.* 2016). It is worth noting that the flow behind the obstacles may be in the inertial or collisional regime, but it is well established that the force on circular objects immersed in granular flows depends solely on the grains that are upstream from the centre of the object (Ding *et al.* 2011).

5. Local flow velocity

What are the roles played by the local flow velocity and local velocity fluctuations around the intruders in the mechanisms responsible for attraction and repulsion? To tackle this question we define square regions where field quantities such as velocity, velocity fluctuations and mass density can be measured. Determining the positions and size that these regions must have is important for making relevant measurements. We define 'in' regions as those that are on the side of the gap between the intruders, and 'out' regions as those that are in between the intruders and the walls (inset in figure 4*a*). This is reasonable, since we were hypothesising

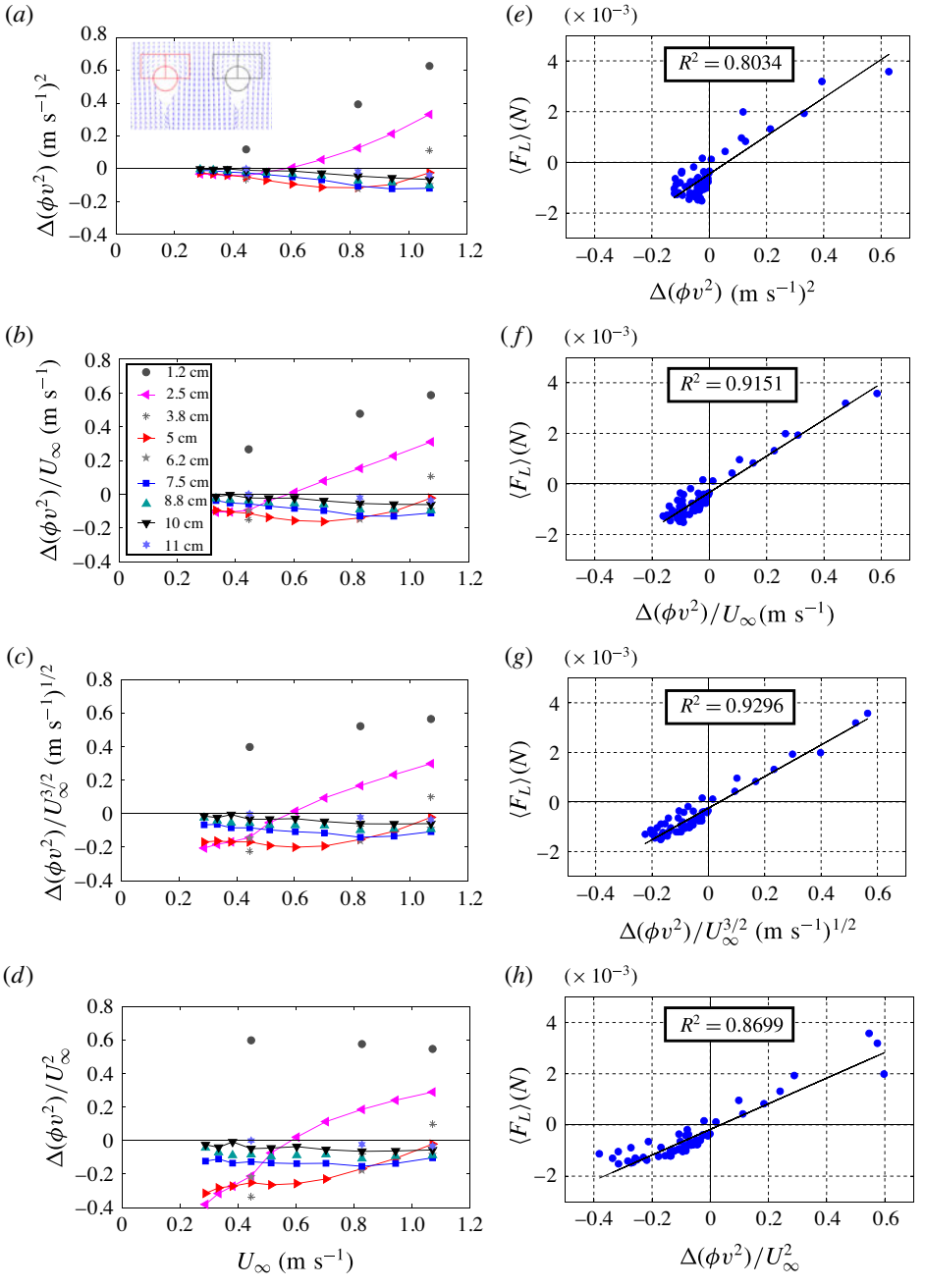

FIGURE 4. (Colour online) (*a–d*) Dependence on flow velocity of the difference in packing fraction times the square of the flow velocity on both sides of the intruders, calculated in the regions adjacent to the upper quadrants of the intruders (see inset in *a*), and divided by a power of the flow velocity with different exponents. (*e–h*) Dispersion of data around the best linear fit in a plot of the average lift force versus $\Delta(\phi v^2)$ divided by the corresponding power of U_∞. It is clear that the expression that best represents $\langle F_L \rangle$, among those tested here, is $\Delta(\phi v^2)/U_\infty^{3/2}$.

that the lift force is related to the difference between the field quantities in the 'in' and 'out' regions. In these regions we measure the mean grain velocity $\langle v(x, y)\rangle = (1/n(x, y, \tau)) \sum_{t=t_1}^{\tau} (\sum_i v_i(x, y))_t$, where $v_i(x, y)$ is the magnitude of the velocity of the ith grain that is inside the region centred at (x, y) at time t, t_1 is the time at which the flow can be considered stationary, τ is the end of the simulation and $n(x, y, \tau)$ is the total number of grains counted on both sums; and we also measure the average mass density $\langle \rho(x, y)\rangle \approx \rho_g \langle \phi(x, y)\rangle_t$, where $\phi(x, y)$ is the area fraction occupied by the grains in the region of measurement at a given time. The difference in the field quantities in the 'in' and 'out' regions that we found useful were $\Delta\langle v\rangle^2 = \langle v(\text{out})\rangle^2 - \langle v(\text{in})\rangle^2$ and $\Delta(\phi v^2) = \langle \phi(\text{out})\rangle\langle v(\text{out})\rangle^2 - \langle \phi(\text{in})\rangle\langle v(\text{in})\rangle^2$. Interestingly, we found that the flows around or below the intruder equator are not related to the forces on the intruder. This finding is consistent with the lift on a single intruder moving horizontally in a granular medium (Ding *et al.* 2011).

Zuriguel *et al.* (2005) suggested that the origin of repulsive lift forces between intruders is a Bernoulli-like effect, where a difference in flow velocity on both sides of the intruders results in a pressure difference with the form $\Delta p = \rho\langle v(\text{out})\rangle^2 - \rho\langle v(\text{in})\rangle^2$. In our system, the quantity $\Delta\langle \phi v^2\rangle$, calculated in the regions adjacent to the upper quadrants of the intruders and plotted versus flow velocity, reproduces the lift force behaviour reasonably well, especially for fast flows and for both repulsion and attraction (figure 4*a*,*e*) (if the quantity $\Delta\langle v^2\rangle$ is plotted instead of $\Delta\langle \phi v^2\rangle$ versus U_∞, the plot does not change substantially; is like multiplying v^2 by a factor of the order of 0.7 (see figure 2 in the supplementary material)). However, the similarity with the lift force is much better when the velocity difference is divided by $U_\infty^{3/2}$ (see figure 4*c*,*g*), which is also better than dividing by U_∞^1 or U_∞^2 (see figure 4). In addition, if measurements are taken in the regions shown in figure 5(*a*), the similarity with the lift force is even better (see figure 5). Therefore, although the difference in the square of the flow velocity between the 'in' and 'out' regions seems to be related to lift force, its relation with pressure does not seem to be solely captured by multiplying by ρ, as suggested by Zuriguel *et al.* (2005). The fact that $\Delta\langle \phi v\rangle^2$ must be divided by $U_\infty^{3/2}$ suggests that the origin of repulsion and attraction is not a Bernoulli effect. As such, we are obliged to conduct a dimensional analysis.

6. Dimensional analysis

Based on the data presented in the previous sections, we propose an equation for the average lift force as follows:

$$\langle F_L\rangle = \frac{f(\mu_{eff})\xi}{Fr^{3/2}} S\Delta(\rho_g \phi v^2) + F_0, \tag{6.1}$$

where f is a dimensionless function of the effective friction coefficient μ_{eff}, $S = dD$ is the relevant obstacle surface, $Fr = U_\infty/\sqrt{gd}$ is the Froude number, $\xi = \xi(h, d, D, L)$ is a dimensionless function that depends on the geometry of the system and F_0 is a function of all the possible variables of the system but varies weakly with X_{sep} and U_∞. By performing variations on h, D and L (see figure 6), we find that, at least as a first-order approximation, the function ξ has the form $\xi = \xi(L, h_{eff}, D^{-3/2})$, where h_{eff} is the effective height of the column above the intruders. Indeed, because of the periodic boundary conditions, the hydrostatic pressure in the granular medium is augmented with respect to the $\rho g h$ value by the pressure exerted by the 'rain' of grains impacting the surface of the granular column after passing the obstacles at the bottom of the cell. This extra pressure can be expressed in the form of a virtual column of height

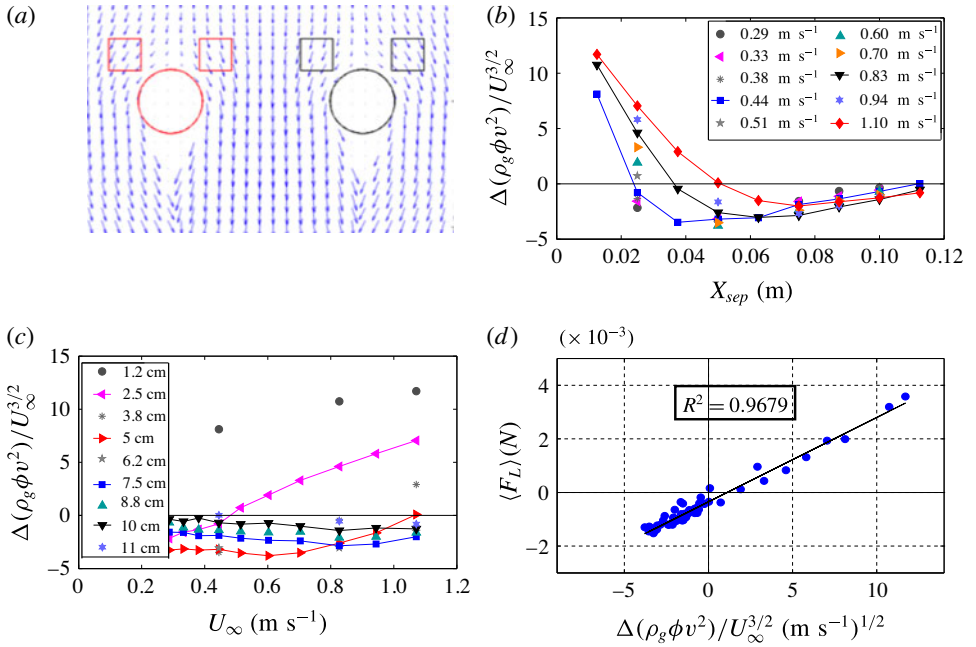

FIGURE 5. (Colour online) (*a*) Regions of measurements found empirically by trial and error where the relation between the field quantities and the lift force were the best. The squares have sides of size $D/2$. (*b*,*c*) Field quantity $\Delta(\rho_g\phi v^2)/U_\infty^{3/2}$ as a function of X_{sep} and U_∞ is very similar to lift force in figure 2. (*d*) Dispersion of data around the best linear fit in a plot of the average lift force versus $\Delta(\rho_g\phi v^2)/U_\infty^{3/2}$. The fit is better than in figure 4(*g*), which shows that the small regions in (*a*) are better than those in figure 4(*a*).

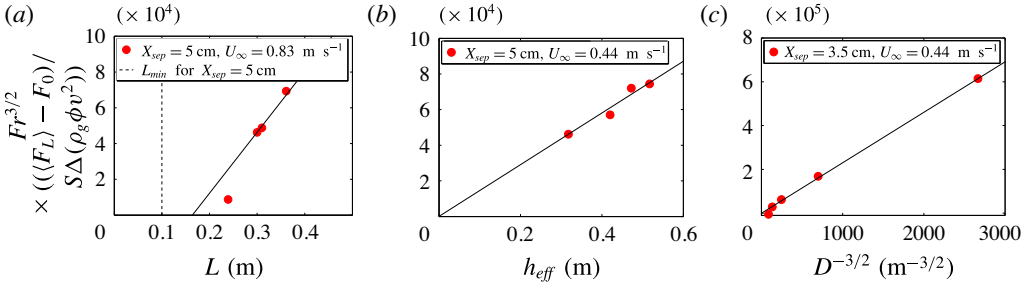

FIGURE 6. (Colour online) Average lift force and local pressure difference $\Delta(\rho_g\phi v^2)$ arranged following (6.1) to study the dependence of ξ on (*a*) L, (*b*) h_{eff} and (*c*) D. The lines are only qualitative guides to the eye to compare data with a linear behaviour. The value of $F_0 = -3.5 \times 10^{-4}$ N was taken from the fit in figure 7(*a*).

$h_r = 13.8$ cm, so that the pressure would be $p_{eff} = \rho g(h + h_r) = \rho g h_{eff}$ with $h_{eff} \sim 48$ cm (see figure 3*b*). With these dimensional constraints, the expression for ξ in (6.1) can be written as

$$\xi = \left(\frac{h_{eff}}{D}\right)\left(\frac{L}{D}\right)\left(\frac{D}{d}\right)^{1/2}. \tag{6.2}$$

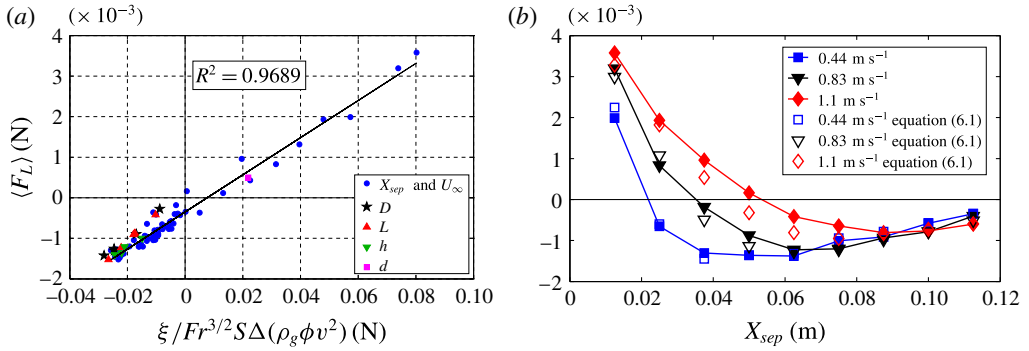

FIGURE 7. (Colour online) (*a*) Dispersion of data around the best linear fit in a plot of the average lift force versus $\xi Fr^{-3/2} S\Delta(\rho_g \phi v^2)$. Most of the data correspond to systematic variations of X_{sep} and U_∞, but the plot also includes data corresponding to variations of D, L, h and d (see figure 1 for their definitions). From the linear fit we get the parameters $f(\mu_{eff}) = 4.6 \times 10^{-2}$ and $F_0 = -3.5 \times 10^{-4}$ N of (6.1). (*b*) Comparison between the average lift force calculated from the force on intruders and the lift force obtained from (6.1) for three different velocities.

When the average lift force is plotted against the term $\xi Fr^{-3/2} S\Delta(\rho_g \phi v^2)$, with ξ given by (6.2), the data follow a better linear pattern than those presented in the previous sections (see figure 7*a*). From the linear fit in figure 7(*a*) we obtain the missing parameters in (6.1): $f(\mu_{eff}) = 4.6 \times 10^{-2}$ and $F_0 = -3.5 \times 10^{-4}$ N. We note that most of the data plotted in figure 7(*a*) correspond to simulations in which systematic variations are made on X_{sep} and U_∞, but the plot also includes simulations where D, L, h and d vary, which demonstrates the robustness of (6.1) and (6.2) as a first-order approximation of those variables.

Figure 7(*b*) shows the average lift force calculated, either directly from the force on intruders, or using (6.1), as a function of X_{sep} for three different velocities. The reproduction of the lift force through the difference in the flow velocity in the 'in' and 'out' regions works remarkably well, although it is not perfect.

There may be a number of reasons for the dispersion of the data observed in figure 7. First, the term F_0 in (6.1) may be a function of all the system variables, although its contribution to the lift force is small. The fact that F_0 varies weakly with X_{sep} and U_∞ indicates that it might stem primarily from intrinsic properties of the granular medium. In addition, negative F_0 means that there exists an attractive lift force even when the local pressure difference given by $\Delta(\rho_g \phi v^2)$ is zero. The origin of this attraction in a symmetric flow remains for the moment as an open question, but we could speculate that fluctuations could play a role here. Second, the expression for the prefactor ξ in (6.2) is an empirical formula that is at best a first-order approximation of the real behaviour. This follows at once from the fact that it is not compatible with the two limiting cases in which the variables become very large or very small. For example, it is clear that the lift force cannot be infinite for a container of infinite width L; instead, it should become saturated at some point, probably following the pressure saturation, such as that described by Janssen in a silo (Pacheco-Vázquez *et al.* 2011). An interesting result in our system is that the lift force changes sign when we double the size of the grains in the medium (see figure 2*d*). This shows a strong dependence of the local flow velocity, the term $\Delta(\rho_g \phi v^2)$, on the size of the grains d. Therefore, the scaling of the lift force as

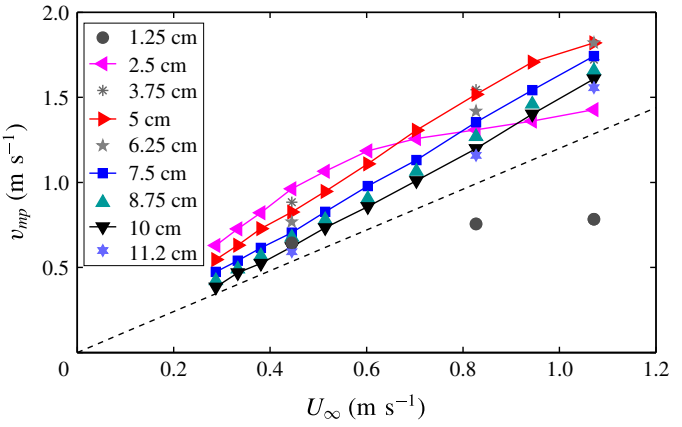

FIGURE 8. (Colour online) Average flow velocity at the middle point between intruders, v_{mp}, plotted as a function of flow velocity U_∞. The dashed line is the average velocity expected from continuity at the middle area of the intruders due to the reduction in the cross-section: $v_{eq} = LU_\infty/(L-2D)$. A comparison with the data in figure 2(*d*) shows that repulsive lift is related to the saturation of v_{mp} due to jamming.

$d^{5/4}$ (almost linear) predicted by (6.1) and (6.2) is probably not the only contribution by d to the lift force. Larger forces for larger grains have been reported on objects dragged horizontally (Albert *et al.* 1999; Ding *et al.* 2011), the result of which is at odds with the observation reported in other work (Chehata *et al.* 2003; Seguin *et al.* 2011), in which the drag on an object immersed in a vertical granular flow increases when the size of the grains decreases. Clearly, the role of grain size on drag and lift forces is not well understood and will require further detailed study. Finally, the linear dispersion of data in figure 7 may also be related to the choice of the regions where the flow is measured, which in our case was determined by trial and error. There is no guarantee that they represent the best choices until an analytical derivation can be made of the relation between lift and local flow.

7. Jamming between intruders

The variation of the average lift force as a function of X_{sep} reveals the competition of two mechanisms, one of which causes attraction and the other repulsion between the intruders. These two regimes are evident in figure 2(*c*), which also shows that the repulsive mechanism is favoured by a small intruder separation and large flow velocities. It has been proposed that the origin of repulsion may be the jamming of particles trying to flow through the gap between intruders (Pacheco-Vazquez & Ruiz-Suarez 2010; Solano-Altamirano *et al.* 2013), but as yet there has been no direct proof. Now, however, with our current set-up, we can support this idea by measuring the average flow velocity at the middle point between the intruders, v_{mp}, and plotting it as a function of U_∞ (figure 8). When we compare this plot with the lift force as a function of U_∞ (figure 2*d*), we observe that whenever v_{mp} varies linearly with U_∞, there is attraction between the intruders, while repulsion is correlated with v_{mp} remaining constant. When the separation between the intruders is 2.5 cm, as in figure 8, the results are especially illustrative in showing how v_{mp} transits from linearity to a constant value when U_∞ increases. This saturation of v_{mp} to a constant value is favoured by small gaps between intruders and by fast flows, as is the case

for the repulsive lift force. Therefore, it is a signature of the jamming of grains trying to flow through the gap between intruders, imposing the maximum possible flow through the gap and pushing apart the intruders, which causes repulsion when U_∞ increases.

What, then, causes attraction? Figure 8 shows that the proximity of the intruders, when jamming has not occurred, accelerates the flow between the intruders and favours attraction. Moreover, the lower the velocity, the stronger the attraction. Therefore, the presence of a neighbour intruder at an intermediate distance facilitates flow in the gap between the intruders, an effect that is enhanced at slow flow velocities. This scenario supports that proposed by Seguin *et al.* (2011), where the drag force on a cylinder penetrating a granular medium can be understood as analogous to a hot cylinder penetrating a fluid whose viscosity decreases when the temperature increases, i.e. when the flow is slow, the temperature between the intruders increases further and the viscosity is at its lowest. This means the extension of the kinetic theory to dense granular flows is a good candidate for describing drag and lift in systems with multiple intruders.

8. Discussion

In summary, we found a strong correlation between the lift force and the difference between local flow velocity and local packing in the 'in' and 'out' regions. The term $\Delta(\rho_g \phi v^2)$ is the same as that found in the lift on an object immersed in a fluid due to the Bernoulli effect. However, the fact that the regions where flow velocity and packing must be measured are not near the middle of the intruders, but in a specific place upstream, suggests that the flow interaction mechanism with the immersed object is not the same as that in a fluid. Besides, the prefactor $Fr^{-3/2} \propto U_\infty^{-3/2}$ is not present in Bernoulli equations. This makes us think that the correlation between $\langle F_L \rangle$ and $\Delta(\rho_g \phi v^2)$ is not necessarily causal, and, based on the fact that the regions of measurement must be upstream from the intruders, we speculate that lift and drag may be related to the local flow around the intruders. A force balance using Coulomb's theory for passive failure, as performed by Ding *et al.* (2011) for the analysis of lift on an object dragged horizontally, may be apt. An extension of kinetic theory to granular flows may also be useful for describing lift and drag in this system (Seguin *et al.* 2011), as would a local rheology model for dense granular flows based on the non-dimensional shear rate I (Andreotti *et al.* 2013). We also found that the range of interaction between intruders, and between intruders and the lateral walls, was much greater than what our experimental set-up allowed us to study due to computational limitations, which explains the strong dependence of the lift force on L (figure 3*a*,*d*) as well as the bizarre result that the drag reduction due to the presence of a neighbour intruder does not change with the separation between intruders (inset in figure 2*c*).

Our system is an excellent set-up for studying the interaction between intruders immersed in a granular flow because measurements are made with the intruders in a stationary state, in contrast to the impact and penetration of objects in a static granular medium that our group studied previously (Solano-Altamirano *et al.* 2013), where depth, pressure and the separation distance between the intruders changed over time. Our motivation for working with static intruders immersed in a granular flow was to develop a better understanding of repulsion and attraction by the impact and penetration of objects in a static granular medium. However, it is not clear now that the results presented here are valid for impact experiments, because when the granular medium is flowing there is agitation in all the grains, which was not present in the

impact experiments. We are currently examining the relation between these two set-ups.

On the other hand, an alternate system that is more closely related to our set-up is a horizontal cylinder half-filled with a granular material, which rotates at different velocities: when big, heavy intruders are immersed in the granular medium and are free to move, they exhibit attractive (repulsive) lift for slow (fast) rotations (Zuriguel *et al.* 2005). It is possible that the regimes of attraction and repulsion described in that work are analogous to the lift force as a function of X_{sep} that we show in figure 2(*c*). However, we do not see any correlation between the lift force and the fluctuations in the velocity of the grains around the intruders, as occurs in the case of the rotating cylinder. We note that our system is two-dimensional, and it has no walls in the third dimension, as it would in experiments. Therefore, it may be that an equivalent three-dimensional experiment would yield a different phenomenology, so it is unclear how valid a comparison would be of the results of our simulations with those of experiments. We are currently performing experiments in a quasi-two-dimensional cell and preliminary results show both repulsion and attraction between intruders, but the role of local flow velocity and velocity fluctuations has not yet been analysed.

9. Conclusions

In conclusion, we studied for the first time the lift and drag of two static intruders placed side-by-side within a granular flow, and observed both attractive and repulsive lift, depending on the separation between the intruders and the flow velocity. The lift force has close correlations with the local flow velocity and packing density around the intruders and we propose an empirical formula that relates these quantities, which should be regarded as a first-order approximation. In addition, we found that the range of the interaction between intruders is much larger than the size of our system, so the dimensional analysis and equations presented here would be valid only for such a situation.

The extent to which our simulations prove useful for understanding real three-dimensional experiments is not yet completely clear, but we are confident that the simplicity of our set-up will attract the interest of many scientists working to advance the understanding of long-range interactions between grains in granular flows.

Acknowledgements

This work has been supported by Conacyt, Mexico, under grant no. 180873. R.A.L.C. thanks Conacyt for financial support. We thank R. Zenit, J. V. Escobar and F. Pacheco-Vázquez for reading and commenting on the manuscript, and we thank J. M. Solano-Altamirano for helping us with the description of the simulations algorithm.

Supplementary material and movies

Supplementary material and movies are available at http://dx.doi.org/10.1017/jfm.2016.384.

REFERENCES

ALBERT, R., PFEIFER, M. A., BARBASI, A. L. & SCHIFFER, P. 1999 Slow drag in a granular medium. *Phys. Rev. Lett.* **82**, 205–208.

ANDREOTTI, B., FORTERRE, Y. & POULIQUEN, O. 2013 *Granular Media: Between Fluid and Solid*. Cambridge University Press.

AUMAÎTRE, S., KRUELLE, C. A. & REHBERG, I. 2001 Segregation in granular matter under horizontal swirling excitation. *Phys. Rev.* E **64**, 041305.

CABALLERO-ROBLEDO, G. & CLÉMENT, E. 2009 Rheology of a sonofluidized granular packing. *Eur. Phys. J.* E **30**, 395–401.

CATTUTO, C., BRITO, R., MARCONI, U. M. B., NORI, F. & SOTO, R. 2006 Fluctuation-induced casimir forces in granular fluids. *Phys. Rev. Lett.* **96**, 178001.

CHEHATA, D., ZENIT, R. & WASSGREN, C. R. 2003 Dense granular flow around an immersed cylinder. *Phys. Fluids* **15**, 1622.

CUNDALL, P. A. & STRACK, O. D. L. 1979 A discrete numerical model for granular assemblies. *Géotechnique* **29** (1), 47–65.

DING, Y., GRAVISH, N. & GOLDMAN, D. I. 2011 Drag induced lift in granular media. *Phys. Rev. Lett.* **106**, 028001.

FAUG, T. 2015 Macroscopic force experienced by extended objects in granular flows over a very broad froude-number range. *Eur. Phys. J.* E **38** (5), 1–10.

GENG, J. & BEHRINGER, R. P. 2005 Slow drag in two-dimensional granular media. *Phys. Rev.* E **71**, 011302.

GOLDMAN, D. I. 2014 Colloquium: biophysical principles of undulatory self-propulsion in granular media. *Rev. Mod. Phys.* **86**, 943–958.

GUILLARD, F., FORTERRE, Y. & POULIQUEN, O. 2014 Lift forces in granular media. *Phys. Fluids* **26** (4), 043301.

GUILLARD, F., FORTERRE, Y. & POULIQUEN, O. 2013 Depth-independent drag force induced by stirring in granular media. *Phys. Rev. Lett.* **110**, 138303.

KIM, I., ELGHOBASHI, S. & SIRIGNANO, W. A. 1993 Three-dimensional flow over two spheres placed side by side. *J. Fluid Mech.* **246**, 465–488.

KNEIB, F., FAUG, T., DUFOUR, F. & NAAIM, M. 2016 Numerical investigations of the force experienced by a wall subject to granular lid-driven flows: regimes and scaling of the mean force. *Comput. Particle Mech.* **3** (3), 293–302.

LEGENDRE, D., MAGNAUDET, J. & MOUGIN, G. 2003 Hydrodynamic interactions between two spherical bubbles rising side by side in a viscous liquid. *J. Fluid Mech.* **497**, 133–166.

MORO, F., FAUG, T., BELLOT, H. & OUSSET, F. 2010 Large mobility of dry snow avalanches: insights from small-scale laboratory tests on granular avalanches of bidisperse materials. *Cold Reg. Sci. Technol.* **62** (1), 55–66.

NELSON, E. L., KATSURAGI, H., MAYOR, P. & DURIAN, D. J. 2008 Projectile interactions in granular impact cratering. *Phys. Rev. Lett.* **101** (6), 068001.

OTTINO, J. M. & KHAKHAR, D. V. 2000 Mixing and segregation of granular materials. *Annu. Rev. Fluid Mech.* **32** (1), 55–91.

PACHECO-VÁZQUEZ, F., CABALLERO-ROBLEDO, G. A., SOLANO-ALTAMIRANO, J. M., ALTSHULER, E., BATISTA-LEYVA, A. J. & RUIZ-SUÁREZ, J. C. 2011 Infinite penetration of a projectile into a granular medium. *Phys. Rev. Lett.* **106**, 218001.

PACHECO-VAZQUEZ, F. & RUIZ-SUAREZ, J. C. 2010 Cooperative dynamics in the penetration of a group of intruders in a granular medium. *Nat. Commun.* **1**, 123.

SANDERS, D. A., SWIFT, M. R., BOWLEY, R. M. & KING, P. J. 2004 Are brazil nuts attractive? *Phys. Rev. Lett.* **93**, 208002.

SEGUIN, A., BERTHO, Y., GONDRET, P. & CRASSOUS, J. 2011 Dense granular flow around a penetrating object: experiment and hydrodynamic model. *Phys. Rev. Lett.* **107**, 048001.

SHAEBANI, M. R., SARABADANI, J. & WOLF, D. E. 2012 Nonadditivity of fluctuation-induced forces in fluidized granular media. *Phys. Rev. Lett.* **108**, 198001.

SOLANO-ALTAMIRANO, J. M., CABALLERO-ROBLEDO, G. A., PACHECO-VÁZQUEZ, F., KAMPHORST, V. & RUIZ-SUÁREZ, J. C. 2013 Flow-mediated coupling on projectiles falling within a superlight granular medium. *Phys. Rev.* E **88**, 032206.

VÉLEZ-CORDERO, J. R., SÁMANO, D., YUE, P., FENG, J. J. & ZENIT, R. 2011 Hydrodynamic interaction between a pair of bubbles ascending in shear-thinning inelastic fluids. *J. Non-Newtonian Fluid Mech.* **166** (1–2), 118–132.

WALTON, O. R. & BRAUN, R. L. 1986 Viscosity, granular-temperature, and stress calculations for shearing assemblies of inelastic, frictional disks. *J. Rheol.* **30** (5), 949–980.

WASSGREN, C. R. 1996 Vibration of granular materials. PhD thesis, California Institute of Technology.

WIEGHARDT, K. 1975 Experiments in granular flow. *Annu. Rev. Fluid Mech.* **7** (1), 89–114.

WIJNGAARDEN, L. V. & JEFFREY, D. J. 1976 Hydrodynamic interaction between gas bubbles in liquid. *J. Fluid Mech.* **77**, 27–44.

WU, J. & MANASSEH, R. 1998 Dynamics of dual-particles settling under gravity. *Intl J. Multiphase Flow* **24** (8), 1343–1358.

ZURIGUEL, I., BOUDET, J. F., AMAROUCHENE, Y. & KELLAY, H. 2005 Role of fluctuation-induced interactions in the axial segregation of granular materials. *Phys. Rev. Lett.* **95**, 258002.